Arch. Metall. Mater. **64** (2019), 2, 457-465

DOI: 10.24425/amm.2019.127560

B. STRAUMAL*,**,***,****#, A. KILMAMETOV**,***, A. GORNAKOVA*, A. MAZILKIN*,***,
B. BARETZKY***, A. KORNEVA*****, P. ZIĘBA*****

DIFFUSIVE AND DISPLACIVE PHASE TRANSFORMATIONS IN NANOCOMPOSITES UNDER HIGH PRESSURE TORSION

The high-pressure torsion (HPT) of Ti-Fe alloys with different iron content has been studied at 7 GPa, 5 anvil rotations and rotation speed of 1 rpm. The alloys have been annealed before HPT in such a way that they contained different amounts of α/α' and β phases. In turn, the β phase contained different concentration of iron. The 5 anvil rotations correspond to the HPT steady-state and to the dynamic equilibrium between formation and annihilation of microstructure defects. HPT leads to the transformation of initial α/α' and β-phases into mixture of α and high-pressure ω-phase. The $\alpha \rightarrow \omega$ and $\beta \rightarrow \omega$ phase transformations are martensitic, and certain orientation relationships exist between α and ω as well as β and ω phases. However, the composition of ω-phase is the same in all samples after HPT and does not depend on the composition of β-phase (which is different in different initial samples). Therefore, the martensitic (diffusionless) transformations are combined with a certain HPT-driven mass-transfer. We observed also that the structure and properties of phases (namely, α-Ti and ω-Ti) in the Ti – 2.2 wt. % Fe and Ti – 4 wt. % Fe alloys after HPT are equifinal and do not depend on the structure and properties of initial α'-Ti and β-Ti before HPT.

Keywords: High-pressure torsion; Ti-Fe alloys; phase transitions; high-pressure phases

1. Introduction

Severe plastic deformation (SPD), in particular one of its modes namely high-pressure torsion (HPT) not only leads to the strong grain refinement [1] but also can drive the phase transformations in the alloys. In other words, the composition and structure of phases after HPT are different from those in the initial state (before HPT). SPD can drive formation [2-4] or decomposition of supersaturated solid solution [5-9], dissolution of precipitates [10-15], amorphization [16-21], nanocrystallization [22-24] etc. In some cases different phase transformations driven by SPD compete with each other and take place simultaneously [18,25]. The majority of such transformations [1-25] is diffusive. In other words, they are connected with the long-range redistribution of the alloy components. If these transitions are driven by SPD they usually include the SPD-driven accelerated mass transfer. Another class of phase transitions is called displacive (or martensitic) ones. Differently to the diffusive phase transitions, the martensitic ones do not include the long-range mass transfer. They involve only short-range atomic displacements. Usually a certain orientation relationship exists between "austenitic" and "martensitic" phases. Recently we observed that SPD can induce not only diffusive phase transitions but also displacive ones [26-30]. Sometimes they proceed simultaneously [31]. The goal of this work is to study the combination of SPD-driven diffusive and displacive phase transformations. For this purpose we have chosen the Ti-based alloys because titanium possesses a high-pressure ω-phase and the $\alpha \rightarrow \omega$ as well as $\beta \rightarrow \omega$ transitions are marternsitic [32-35]. We chosen the Ti-Fe alloys for our studies because iron is one of the most common alloying components in the titanium alloys, among the so-called β-stabilisers. One of the important reasons is that iron is the most cheap among others alloying components in Ti-alloys. Also, the SPD can provide the unique mechanical properties of Ti and Ti-based alloys [36-38]. Thus, one achieved the unusual combination of high strength and ductility in nanograined SPD-Ti [39].

2. Experimental

We investigated in this work the Ti – 2.2 wt. % Fe, Ti – 4 wt. % Fe and Ti – 10 wt. % Fe alloys produced of high purity components (99.9% Ti and 99.97% Fe) with the inductive melting. The melt was poured in vacuum into the water-cooled cylindrical copper crucible of 10 mm diameter. The 0.7 mm thick discs were cut from ingots and individually sealed in the evacuated silica

* RUSSIAN ACADEMY OF SCIENCES, INSTITUTE OF SOLID STATE PHYSICS, CHERNOGOLOVKA, RUSSIA
** RUSSIAN ACADEMY OF SCIENCES, SCIENTIFIC CENTER IN CHERNOGOLOVKA, CHERNOGOLOVKA, RUSSIA
*** KARLSRUHE INSTITUTE OF TECHNOLOGY (KIT), INSTITUTE OF NANOTECHNOLOGY, EGGENSTEIN-LEOPOLDSHAFEN, GERMANY
**** NATIONAL UNIVERSITY OF SCIENCE AND TECHNOLOGY «MISIS», MOSCOW, RUSSIA
***** INSTITUTE OF METALLURGY AND MATERIALS SCIENCE, POLISH ACADEMY OF SCIENCES, 25 REYMONTA STR. 25, 30-059 CRACOW, POLAND
# Corresponding author: straumal@issp.ac.ru

ampoules with residual pressure of 4×10^{-4} Pa. The ampoules with samples inside have been annealed at $T = 950$ °C, 104 h, $T = 800$ °C, 270 h, $T = 680$ °C, 550 h and $T = 620$ °C, 270 h, i.e. in β and $\alpha + \beta$ areas of the Ti-Fe phase diagram (see squares in Fig. 1a). After annealing the samples were quenched in water at room temperature (without breaking the ampoules). Afterwards the disks were deformed by HPT in a Bridgman anvil type unit using a custom built computer-controlled device manufactured by W. Klement GmbH, Lang, Austria. HPT took place at room temperature, pressure of 7 GPa, with the speed of 1 rotation-per-minute and 5 anvil rotations. The temperature of the sample increases during HPT only negligible, up to about 40-50 °C. The HPT machine permitted to measure the torsion torque during HPT. The torsion torque increased during 1-2 anvil rotations in all alloys and pure Ti and then remained almost unchanged (Fig. 2). In other words, the torsion torque reached a steady state as it has been observed previously in other alloys in Refs. [5-9,25,36]). The central low-deformed part of each disk (about 3 mm in diameter) was excluded after HPT from further investigations.

X-ray diffraction (XRD) patterns were obtained in the Bragg-Brentano geometry in a powder diffractometer (Philips X'Pert) with Cu-Kα radiation. The scan speed for XRD analysis was about 2 deg/min. The Pseudo-Voigt function was used for fitting of XRD peak profiles. Lattice parameters were evaluated by the Fityk software [41] using a Rietveld-like whole profile refinement. Relative amount of α, β and ω phases was estimated basing on the comparison of the integrated intensities with an error of about ±2-3%. Pure polycrystalline titanium was used

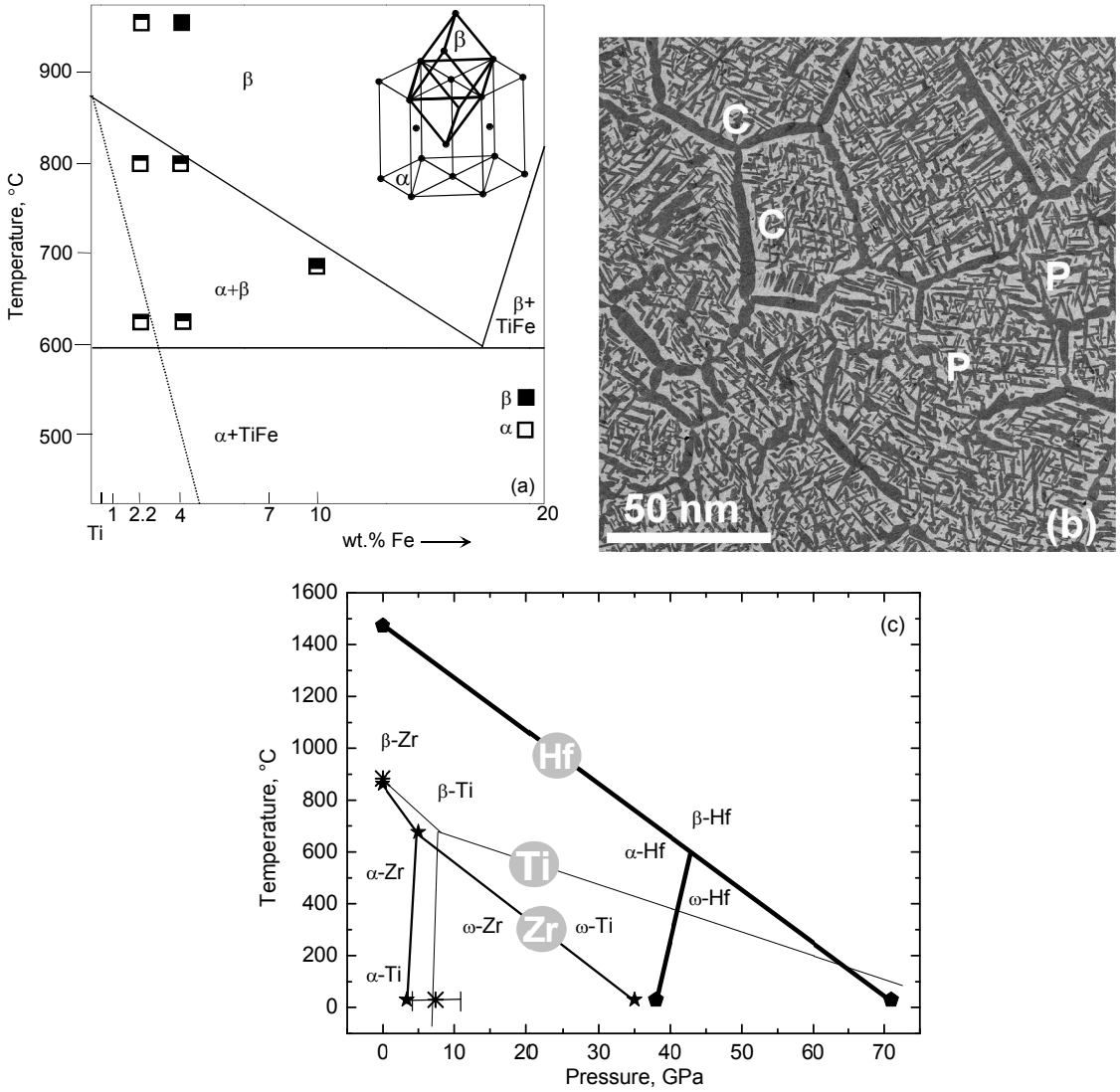

Fig. 1. (a) Ti-rich corner of the Ti-Fe phase diagram with calculated T_0-line for martensitic transformation (dotted line). The black and white areas of the boxes show roughly the ratio between β and α/α' phases, respectively, in samples after annealing and quenching. Inset: orientation relationship between β-Ti and α/α'-Ti. (b) SEM micrograph of Ti – 4 wt.% Fe alloy after annealing at 620 °C and quenching. α-phase appears dark and β-phase appears bright. The α-phase form continuous (marked with letter C) or discontinuous (marked as P) layers in β/β grain boundaries. Continuous GB layers correspond to the complete wetting of β/β GBs by a second solid phase α. Discontinuous GB layers correspond to the partial wetting of β/β GBs by a second solid phase α. (c) A "Temperature – pressure" equilibrium phase diagram for titanium (crosses, thin lines), zirconium (stars, middle-thick lines) and hafnium (pentagons, thick lines). Error bar reflects the scatter of experimental data for the pressure of α-ω transformation at room temperature

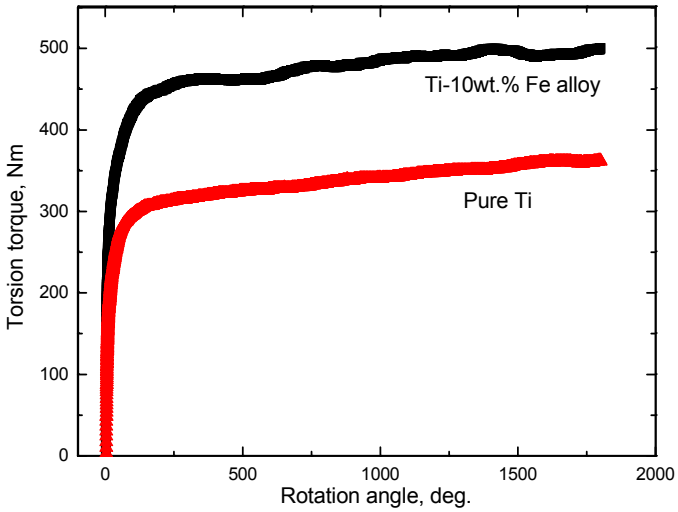

Fig. 2. Dependence of the torsion torque during HPT on the rotation angle for (a) pure titanium (bottom curve, red) and Ti – 10 wt. % Fe alloy (top curve, black)

as reference. An empirical rule known as Vegard's rule (1921) was taken into account for subsequent analysis. SEM studies have been done using the Tescan Vega TS5130 MM microscope equipped with the LINK energy-dispersive X-Ray spectrometer (Oxford Instruments). Transmission electron microscopy (TEM) and high resolution TEM (HRTEM) observations have been made by using an aberration corrected TITAN 80-300 transmission electron microscope. The cross section TEM and HRTEM specimens were cut from HPT discs at a 3 mm distance from the disc center. They were further thinned in a FEI Strata 400S dual beam facility. Automated Crystal Orientation Mapping (ACOM) TEM technique was used for phase mapping in the alloys after the HPT deformation. The ACOM TEM measurements were carried out on a Philips Tecnai F20ST operated at 200 kV in microprobe STEM mode. NanoMegas ASTAR system was used for ACOM-TEM data acquisition [42]. A primary electron beam with about 1 nm diameter and a convergence semi-angle of 1.4 mrad was generated. A camera length of 80 mm was used to acquire the diffraction patterns [43]. For indexing of the collected ACOM TEM diffraction patterns, we took the lattice parameters of the phases evaluated from the X-rays diffraction (XRD) data. Radial intensity distribution in ACOM TEM diffraction patterns was calculated using the ProcessDiffraction soft package [44].

3. Results

In Fig. 1a the Ti-rich corner of Ti-Fe phase diagram [40] with calculated T_0-line for martensitic transformation is shown. Squares mark the annealing temperatures and schematically show different phase in Ti-Fe samples after annealing and quenching. After anneaing the samples contained different amount of α/α' and β phases, in turn, the β phase contained different concentration of iron. In the samples with low Fe-content (below 4 wt.% Fe) annealed in the one-phase β-area and quenched, the martensite transformation of β-phase into α' martensite takes place [32]. Orientation relationship $(0001)_\alpha \| (110)_\beta$; $\langle 11\bar{2}0\rangle_\alpha \| \langle 111\rangle_\beta$ between β-Ti and α/α'-Ti is shown in the inset in Fig. 1a [41-50]. The amount of α'-martensite was maximal in the samples with 0.5 wt.% Fe [32]. The Ti – 4 wt. % Fe alloy quenched from 950 °C contains almost 100% of undercooled β-phase. All other annealed and quenched Ti-Fe alloys consist of the mixture of α/α' and β phases in different ratios. Moreover, the samples annealed in the two-phase $\alpha + \beta$ area of the Ti-Fe phase diagram contain the α-phase with almost zero concentration of iron and β-phase which accommodates the iron present in the individual sample. The annealed β-phase can contain up to 17 wt.% Fe, according to the α-to-β transus line in the Ti-Fe phase diagram (Fig. 1a). Fig. 1b shows SEM micrograph of Ti-10 wt.% Fe alloy after annealing at 680 °C and quenching. α-phase appears dark and β-phase appears bright. After annealing the grain size in samples before HPT was several hundreds of μm. The α-phase forms short small stripe-like precipitates within the large grains. It forms also continuous (marked with letter C) or discontinuous (marked with letter P) layers in β/β grain boundaries. This corresponds to the complete (C) or partial (P) wetting of β/β GBs by a second solid phase α [36,86-88].

Figure 1c shows the temperature-pressure equilibrium phase diagram comparison for pure titanium, zirconium and hafnium. Contrary to the pure titanium, the ω-phase was observed in various Ti-based alloys even at ambient pressure after quenching or isothermal ageing [51,52]. However, in our experiments an extremely small amount of ω-phase was observed only in few annealed and quenched Ti-Fe samples.

Figure 2 shows the dependence of torsion torque during HPT on the anvil rotation angle for pure titanium (bottom curve, red) and Ti – 10 wt. % Fe alloy (top curve, black). The torsion torque substantially grows up with the increase in anvil rotation angle. However, after 0.5-1 rotation it reaches a certain saturation slowly approaching a steady-state value. As one can expect, the Ti – 10 wt. % Fe alloy is much stronger than pure Ti (because of the solid solution/precipitation hardening). Its value of steady-state torsion torque (500 N·m) is higher in comparison to that for pure titanium (350 N·m). Therefore, we investigated the structure of Ti-Fe alloys after HPT "deep" in the steady-state after 5 anvil rotations (1800 deg.). Fig. 3 shows the orientation relationship between the lattices of β- and ω-phases [51,52].

Figure 4a shows the XRD patterns for the Ti – 2 wt. % Fe alloy annealed at T = 950 °C, 104 h (top plot), T = 800 °C, 270 h (middle plot) and T = 620 °C, 270 h (bottom plot) after annealing and quenching before HPT. Fig. 4b shows the XRD patterns for the same samples after HPT. The patterns are vertically shifted for better comparison. The samples before HPT (Fig. 4a) contain the mixture of α'- and β-phases. α'-phase is the martensite containing the higher amount of iron than equilibrium α-phase [32]. The amount of α'-phase increases with decreasing annealing temperature. The position of α'-peaks remain almost the same. The peaks of β-phase move towards higher diffraction angles with decreasing annealing temperature. It means that the concentration of iron in the β-phase increases because the addi-

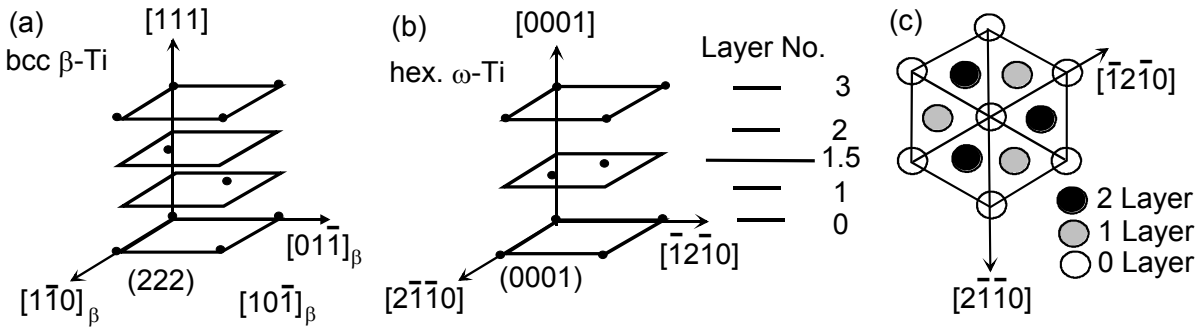

Fig. 3. Orientation relationship between β-Ti and ω-Ti. Planar arrangement of the $\{222\}_\beta$ atomic planes in the bcc lattice; (a) the ABCABC… sequences of atomic plane arrangements could be noticed (planes are marked as 0,1,2,3). (b) The planar arrangement of the $(0001)_{\omega\_}$ atomic planes in the ω-lattice. Thus, the ω-lattice could be obtained from the bcc lattice by collapsing a pair of planes (1 and 2, as shown in figure) in the middle (marked as 1.5) while keeping the third one (0 and 3) undisturbed. (c) Completely collapsed {222} planes form a sixfold symmetry whereas an incomplete collapse forms a threefold symmetry along the <111> axis [52]

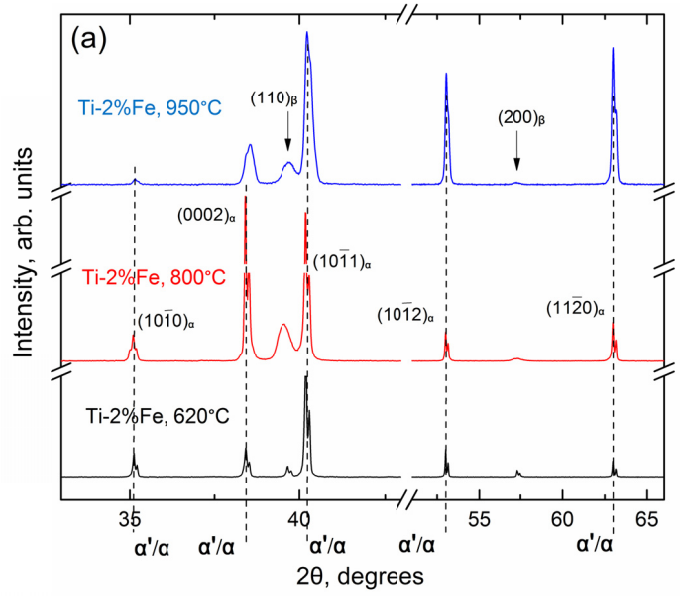

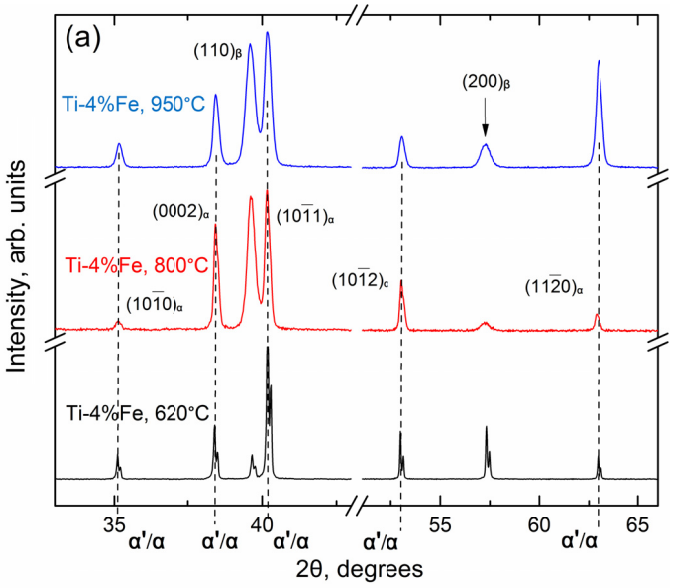

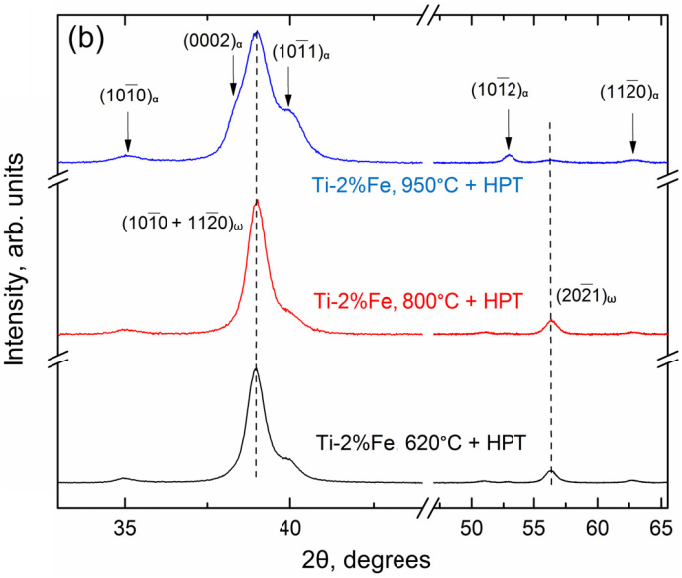

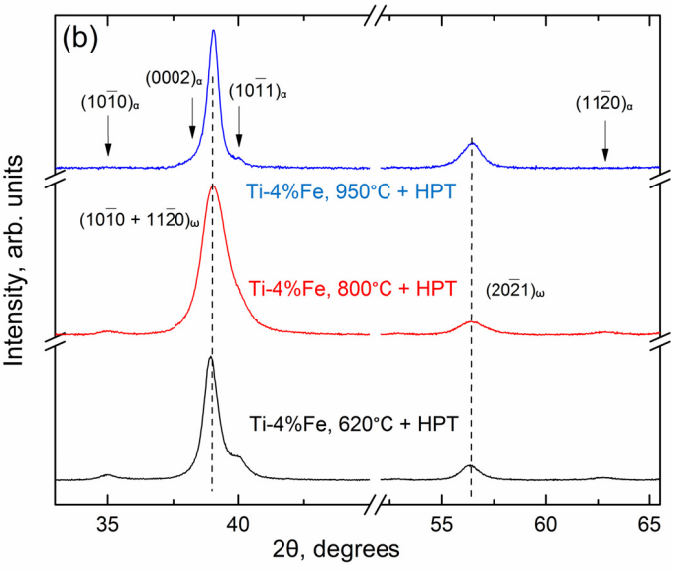

Fig. 4. The X-ray diffraction patterns of the Ti – 2 wt. % Fe alloy annealed at T = 950 °C, 104 h (top plot), T = 800 °C, 270 h (middle plot) and T = 620 °C, 270 h (bottom plot) in the state after annealing and quenching (a) and after HPT at 7 GPa, 1 rpm, 5 rot (b). The patterns are vertically shifted for better comparison

Fig. 5. The X-ray diffraction patterns of the Ti – 4 wt. % Fe alloy annealed at T = 950 °C, 104 h (top plot), T = 800 °C, 270 h (middle plot) and T = 620 °C, 270 h (bottom plot) in the state after annealing and quenching (a) and after HPT at 7 GPa, 1 rpm, 5 rot (b). The patterns are vertically shifted for better comparison

tion of iron decreases the lattice parameter of β-phase [33,53-56]. The peaks of β-phase are rather broad. It is due to the small size of β-grains distributed among the large α'-grains. The samples after HPT (Fig. 4b) contain mainly ω-phase (about 85 %) and a little α-phase. HPT destroys the α'-martensite with increased Fe content and forms the almost equilibrium α-phase with less iron inside [32]. The X-rays patterns are almost identical for all three samples.

Figure 5a shows the XRD patterns for the Ti – 4 wt. % Fe alloy annealed at T = 950 °C, 104 h (top plot), T = 800 °C, 270 h (middle plot) and T = 620 °C, 270 h (bottom plot) after annealing and quenching before HPT. Figure 5b shows the XRD patterns for the same samples after HPT. The patterns are vertically shifted for better comparison. The annealed at T = 950 °C and quenched Ti – 4 wt. % Fe alloy (Fig. 5a, top curve) has only β-phase and low amount of α'-phase (martensite). The β-phase contains 4 wt. % Fe i.e. as much as the total iron concentration in the whole sample. The sample Ti – 4 wt. % Fe annealed at T = 800 °C and quenched (Fig. 5 middle curve) contained α-phase with very low iron content and β-phase with a high Fe concentration. The iron content in the Ti – 4 wt. % Fe sample annealed at T = 620 °C is even higher. The volume ratio of α- and β-phases corresponds to the phase Ti-Fe diagram at 800 °C and 620 °C (Fig. 1a). Iron addition decreases the lattice constant of β-phase [53-56], therefore β-peaks in Fig. 5a (middle and bottom curves) are shifted to the right in comparison to β-peaks in Fig. 5a (top curve). The peaks of β-phase in samples quenched from high temperature are rather broad. It is due to the small size of β-grains distributed among the large α'-grains.The samples after HPT (Fig. 5b) contain mainly ω-phase (about 95%) and a little α-phase. The X-rays patterns are almost identical for all three samples.

In Figure 6 the HREM micrograph of the Ti-4 wt. % Fe alloy after HPT is shown. Corresponding FFTs shows coexistence of β and ω-phases with orientation relationship, so that $[110]_\beta \| [124]_\omega \| [100]_\omega$. Reflexes from the plane with FN = $[100]_\omega$ are shown by arrows.

4. Discussion

In Fig. 1b the equilibrium "temperature-pressure" phase diagram for pure titanium is shown obtained by *in situ* experiments under hydrostatic pressure [51,57-66]. In pure titanium, the high-pressure phase transition from α-phase to ω-phase takes place [51,57,59-61,63-66]. At room temperature, it occurs between 2.9 and 10.5 GPa, depending on the experimental technique, on the pressure environment, and on the sample purity (this pressure range is shown by vertical dotted lines at 2.9 and 10.5 GPa) [51,59,63-66]. The triple point α-ω-β was experimentally determined at 640 °C and 7.5 GPa [65]. The low temperature α-titanium crystallizes in the hexagonal close packed (hcp) crystal structure (space group $P6_3/mmc$, Wyckoff positions 2c) with the ratio of the lattice parameters $c/a \approx 1.58$. Above 882 °C, the body centred cubic (bcc) β-Ti is stable, which crystallizes in the space group $Im\bar{3}m$, where the Ti atoms occupy the Wyckoff positions 2a. The crystal structure of ω-Ti is hexagonal (space group P6/mmm), and the Ti atoms occupy the Wyckoff positions 1*a* and 2*d* [58, 63]. The crystallographic mechanism of the $\alpha \leftrightarrow \omega$ (or $\alpha \leftrightarrow \beta \leftrightarrow \omega$) phase transformation under equilibrium conditions (i.e. without external shear) was described in Refs [58,63]. It was suggested in [63] that the $\alpha \rightarrow \omega$ transformation at low temperatures proceeds through β-Ti as $\alpha \rightarrow \beta \rightarrow \omega$, although β-Ti in pure titanium is thermodynamically unstable below 882 °C. The $\alpha \rightarrow \omega$ transformation is of martensitic-type and characterized by a rather large pressure hysteresis, thus the ω-phase can be retained in the material after the release of the pressure [61].

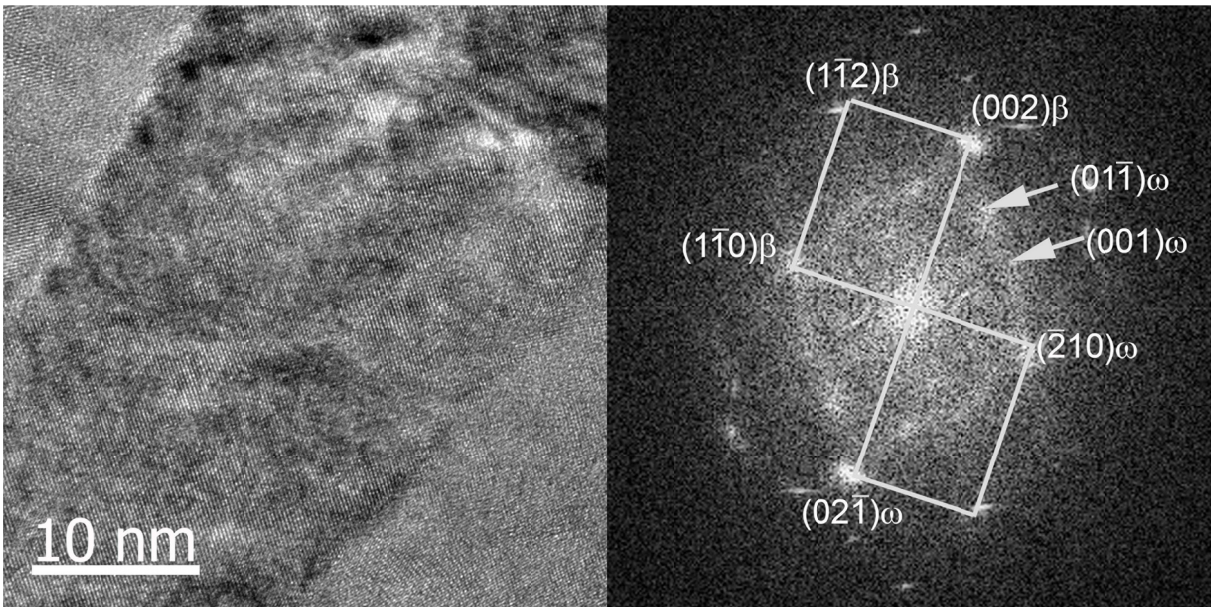

Fig. 6. HREM micrograph of the Ti – 4 wt. % Fe alloy. Corresponding FFTs shows coexistence of β and ω-phases with orientation relationship, so that $[110]_\beta \| [124]_\omega \| [100]_\omega$. Reflexes from the plane with FN = $[100]_\omega$ are shown by arrows

The lattice relationship (Fig. 3) between the β- and the ω -structures does not only establish the crystal structure of the ω -phase but also provides a clue to the transformation mechanism. The orientation relationship between the two phases has been determined in a large number of investigations and has been unanimously described as [50,52]:

$$\{111\}_{\beta}\|(0001)_{\omega};\langle 1\bar{1}0\rangle_{\beta}\|\langle 11\bar{2}0\rangle_{\omega}$$

This orientation relationship between β- and the ω-phases is clearly seen in Fig. 6 where the HREM micrograph of the Ti – 4 wt. % Fe alloy after HPT is shown. Thus, the martensitic (diffusionless) transformation proceeds indeed during HPT.

The ω-phase exists not only in pure titanium as high-pressure stable phase. It appears also in titanium alloys. In particular, the ω-phase can also exist as a metastable phase in titanium alloyed with transition elements [67-75]. The metastable phases in titanium alloys with transition elements are classified as electron-type ones and their formation is associated with a specific concentration of ($s + d$)-electrons per atom [100]. In general case (depending on the concentration of the alloying element in the alloy, the heat treatment, or the production mode) one can speak of the following metastable phases of the type: commensurate ω-phase (or athermal), incommensurate (or diffusional) ω-phase, quasi-crystalline phases, and their approximants [67,68]. Commensurate ω-phase can form during quenching of a high-temperature bcc solid solution (β-phase) in a rather narrow concentration range corresponding to electron concentration $C = 4.1 – 4.2$ electrons/atom [69-72]. It has a rhombohedral crystal structure with a ratio of lattice periods $c/a = 0.612$ [67]. The $\beta \rightarrow \omega$ transformation occurs by some displacements of atoms from neighbor planes {111} of the initial bcc lattice over the direction [111] toward each other to distances not exceeding interatomic ones (see scheme in Fig. 3) [102,103]. The phase known as an incommensurate or diffusion ω-phase forms after quenching from the β-region in titanium alloys with higher concentration of the alloying element than that corresponding to the formation of commensurate ω-phase [73-75].

Various orientation relationships (ORs) exist between α, α', β and ω phases.

β- and α'-phases: $(0001)_{\alpha}\|(110)_{\beta}$; $\langle 11\bar{2}0\rangle_{\alpha}\|\langle 111\rangle_{\beta}$ [41-49],

β- and ω-phases: $\{111\}_{\beta}\|(0001)_{\omega}$; $\langle 1\bar{1}0\rangle_{\beta}\|\langle 11\bar{2}0\rangle_{\omega}$ [50,52],

α- and ω-phases: OR 1 $(0001)_{\alpha}\|(01\bar{1}1)_{\omega}$; $\langle 11\bar{2}0\rangle_{\alpha}\|\langle 1\bar{1}01\rangle_{\omega}$

and OR 2 $(0001)_{\alpha}\|(11\bar{2}0)_{\omega}$; $\langle 11\bar{2}0\rangle_{\alpha}\|\langle 0001\rangle_{\omega}$ [58]

These ORs make commensurate the lattices of phases before and after phase transition. This make also possible the martensitic mechanism of transition, just by shear, i.e. without diffusive mass-transfer. In martensitic transformations each atom after transformation usually remains surrounded by the same neighbors as before transformation. The alloying of titanium changes the lattice spacing of "austenite" and "martensite" phases [52]. Therefore, it can facilitate (or obstruct) the martensitic transformations. It is because the alloying differently changes the lattice spacing of "austenite" and "martensite" phases. As a result, after addition of alloying atoms, the lattices of phases can match each other better than in pure Ti. Moreover, the HPT-driven mass-transfer can redistribute the atoms of alloying component, improve the lattice matching and, thus, facilitate the martensitic transformations.

The evaluation of the lattice parameters for ω-phase enables to estimate the input of Fe content to the changes of the atomic volume per unit cell of this phase. After HPT of Ti – 4 wt.% Fe alloy, both lattice parameters of ω-phase appeared to be maximally reduced ($a = 0.4610$ nm, $c = 0.2825$ nm) in comparison to the ω phase in commercially pure HPT Ti ($a = 0.4627$ nm, $c = 0.2830$ nm). The corresponding reduction of the atomic volume achieves the value of 0.9%, which is comparable, for example, to the difference between α- and β-phase atomic volumes. Consequently, the calculated atomic density of the ω-phase shows its maximum around 4 wt.% Fe concentration and nicely correlates with the atomic density for β-phase estimated from the literature data for the same Fe content [33]. Indeed, assuming lattice parameter $a_{\beta} \approx 0.326$ nm for 4 wt.% Fe [76,78] one can obtain the atomic density equal to 57.73 at/nm^3. This correlation appears to be in a good agreement with the optimal condition for the HPT-induced ω-phase formation [33].

The ω-phase is known as the most dense crystallographic structure among other modifications of titanium, and formation of its metastable state is closely associated with the specific electron structure. When an external perturbation, such as pressure, significantly changes an atomic volume, shorter bonds always have a larger effect on the orbital occupancy than the longer ones [78]. If the atoms get closer, not only p- and s-bands are further broadened, but also d-bands become dispersive, and different orbitals start to share the same electronic states, i.e. orbital hybridization starts. Orbital hybridization itself is necessary to maximize the strength of the interatomic bonds by optimizing the direction and overlap of the atomic orbitals in the given crystallographic structure. In our case, the shortest interatomic bonds in the ω-phase are revealed for 4 wt.%Fe alloying. Taking into account that this solid solution corresponds to maximal volume fraction of ω-phase [33], one can consider the ω-phase with 4 wt.%Fe as the most stable state created by HPT treatment. Further increase in alloying with Fe leads to lower stability of ω-phase and, opposite, to higher stability of β-phase [33]. This assumption is consistent with the reported value, equal to 5 at.%Fe, of minimum concentration of the alloying for the complete stabilization of the β-phase [79,80].

In previous works we observed that the composition and structure of phases during HPT in the steady-state condition is controlled by the dynamic equilibrium between defect formation during SPD and defect relaxation [5,8,25]. Also, the extremely high concentration of vacancies was observed at the steady-state during HPT [53,54,81,82]. We observed also that in many cases the composition and structure of phases during HPT at this steady-state is a function of HPT conditions (temperature, pressure, strain rate) and does not depend on the starting state

of the sample before HPT (for example, the composition and morphology of phases). Thus, such steady-state is a kind of *attractor* and following von Bertalanffi can be called *equifinal* [83]. The closed systems tend to evolve towards *equilibrium* state independent of starting state. Similarly, the opened systems tend to seek the sustained *equifinal* state, also independent of starting one [83].

Such *"equifinality"* appears also in our case. For example, we studied three different starting states for the samples containing 2.2 and 4 wt.% Fe. As we mentioned above, 4 wt.% Fe is the optimum concentration for the lattice matching between β- and ω-phases. After annealing at 950 °C in the one-phase β area of the Ti-Fe phase diagram and quenching the alloy contained solely β-phase (Fig. 5a, top curve). The $\beta \rightarrow \omega$ transition proceeds in this sample completely and very quickly. Already after 0.1 rot. the sample contained almost only ω-phase [33]. It is because no mass transfer is needed for the $\beta \rightarrow \omega$ transition, and is can proceed via martensitic or diffusionless mechanism.

To the opposite, the Ti – 4 wt.% Fe samples annealed at 800 °C and 620 °C, namely in the two-phase $\alpha + \beta$ area of the Ti-Fe phase diagram, and quenched contained the mixture of α- and β-phases (Fig. 5a, middle and bottom curves). In full accordance with the phase diagram, the α-phase in such samples is almost free from iron, and all iron atoms are diluted in β-phase, which contains much more iron than 4 wt.% Fe. As a result, if the sample contains a mixture of α- and β-phases, mass transfer is needed for the $\beta \rightarrow \omega$ transition, and ω-phase appears only after significant strain [33]. This diffusion-like mass transfer proceeds extremely quick, the estimated equivalent diffusion coefficients are 10-15 orders of magnitude higher than the bulk diffusion coefficient extrapolated to 300 K (being the HPT temperature) [33]. And it despite to the fact that the applied pressure additionally slows down the diffusion [84, 85].

Nevertheless, after five anvil rotations (i.e. "deep" in the steady state, see Fig. 2) the state in all three samples is the same, independently on the starting state. They contain almost 95% of ω-phase (Fig. 5b). Similar behavior we observed also for the alloy with 2 wt.% Fe (Fig. 4). Thus, after HPT the amount of α- and ω-phases is the same in all three samples, as well as the composition of these phases. Therefore, the state after 5 anvil rotation can be determined as *"equifinal"*.

5. Conclusions

The high-pressure torsion (HPT) of Ti-Fe alloys with different iron content, different amounts of α/α' and β phases in the initial state as different composition of α/α' and β phases has been studied. The 5 anvil rotations correspond to the HPT steady-state and to the dynamic equilibrium between formation and annihilation of microstructure defects. HPT leads to the transformation of initial α/α' and β-phases into mixture of α and high-pressure ω-phase. The $\alpha \rightarrow \omega$ and $\beta \rightarrow \omega$ phase transformations are martensitic, and certain orientation relationships exist between α and ω as well as β and ω phases. Therefore, the martensitic (diffusionless) transformations are combined with a certain HPT-driven mass-transfer. The structure and properties of α-Ti and ω-Ti phases after HPT are equifinal and do not depend on the structure and properties of initial α'-Ti and β-Ti before HPT.

Acknowledgements

This work was partially supported by Ministry of Education and Science of the Russian Federation in the framework of the Program to Increase the Competitiveness of NUST "MISiS", the National Science Centre of Poland (grant OPUS, DEC-2017/27/B/ST8/01092), the state task of ISSP RAS and SCC RAS, by the Russian Foundation for Basic Research (grants 16-03-00285, 16-53-12007 and 18-03-00067), by Deutsche Forschungsgemeinschaft (project numbers RA 1050/20-1, IV 98/5-1, HA 1344/32-1, FA 999/1-1) as well as by the Karlsruhe Nano Micro Facility (KNMF, www.knmf.kit.edu).

REFERENCES

[1] R.Z. Valiev, R.K. Islamgaliev, I. Alexandrov, Progr. Mater. Sci. **45**, 103 (2000).

[2] W. Lojkowski, M. Djahanbakhsh, G. Burkle, S. Gierlotka, W. Zielinski, H.J. Fecht, Mater. Sci. Eng. A **303**, 197 (2001).

[3] V.G. Gavriljuk, Mater. Sci. Eng. A **345**, 81 (2003).

[4] X. Sauvage, F. Wetscher, P. Pareige, Acta Mater. **53**, 2127 (2005).

[5] B.B. Straumal, B. Baretzky, A.A. Mazilkin, F. Phillipp, O.A. Kogtenkova, M.N. Volkov, R.Z. Valiev, Acta Mater. **52**, 4469 (2004).

[6] A.A. Mazilkin, B.B. Straumal, E. Rabkin, B. Baretzky, S. Enders, S.G. Protasova, O.A. Kogtenkova, R.Z.Valiev, Acta Mater. **54**, 3933 (2006).

[7] B.B. Straumal, S.G. Protasova, A.A. Mazilkin, E. Rabkin, D. Goll, G. Schütz, B. Baretzky, R. Valiev, J. Mater. Sci. **47**, 360 (2012).

[8] B.B. Straumal, A.R. Kilmametov, Yu.O. Kucheev, L. Kurmanaeva, Yu. Ivanisenko, B. Baretzky, A. Korneva, P. Zięba, D.A. Molodov, Mater. Lett. **118**, 111 (2014).

[9] B. Straumal, R. Valiev, O. Kogtenkova, P. Zieba, T. Czeppe, E. Bielanska, M. Faryna, Acta Mater. **56**, 6123 (2008).

[10] C.M. Cepeda-Jiménez, J.M. García-Infanta, A.P. Zhilyaev, O.A. Ruano, F. Carreño, J. Alloys Comp. **509**, 636 (2011).

[11] Y. Ivanisenko, W. Lojkowski, R.Z. Valiev, H.J. Fecht, Acta Mater. **51**, 5555 (2003).

[12] B.B. Straumal, A.A. Mazilkin, S.G. Protasova, S.V. Dobatkin, A.O. Rodin, B. Baretzky, D. Goll, G. Schütz, Mater. Sci. Eng. A **503**, 185 (2009).

[13] V.V. Sagaradze, V.A. Shabashov, Nanostruct. Mater. **9**, 681 (1997).

[14] S. Ohsaki, S. Kato, N. Tsuji, T. Ohkubo, K. Hono, Acta Mater. **55**, 2885 (2007).

[15] B.B. Straumal, S.V. Dobatkin, A.O. Rodin, S.G. Protasova, A.A. Mazilkin, D. Goll, B. Baretzky, Adv. Eng. Mater. **13**, 463 (2011).

[16] A.V. Sergueeva, C. Song, R.Z. Valiev, A.K. Mukherjee, Mater. Sci. Eng. A **339**, 159 (2003).
[17] S.D. Prokoshkin, I.Yu. Khmelevskaya, S.V. Dobatkin, I.B. Trubitsyna, E.V. Tatyanin, V.V. Stolyarov, E.A. Prokofiev, Acta Mater. **53**, 2703 (2005).
[18] X. Sauvage, L. Renaud, B. Deconihout, D. Blavette, D.H. Ping, K. Hono, Acta Mater. **49**, 389 (2001).
[19] T. Miyazaki, D. Terada, Y. Miyajima, C. Suryanarayana, R. Murao, Y. Yokoyama, K. Sugiyama, M. Umemoto, T. Todaka, N. Tsuji, J. Mater. Sci. **46**, 4296 (2011).
[20] A.A. Mazilkin, G.E. Abrosimova, S.G. Protasova, B.B. Straumal, G. Schütz, S.V. Dobatkin, A.S. Bakai, J. Mater. Sci. **46**, 4336 (2011).
[21] B.B. Straumal, A.A. Mazilkin, S.G. Protasova, D. Goll, B. Baretzky, A.S. Bakai, S.V. Dobatkin, Kovove Mater. – Metall. Mater. **49**, 17 (2011).
[22] A.M. Glezer, M.R. Plotnikova, A.V. Shalimova, S.V. Dobatkin, Bull. Russ. Ac. Sci. Phys. **73**, 1233 (2009).
[23] G.E. Abrosimova, A.S. Aronin, S.V. Dobatkin, S.D. Kaloshkin, D.V. Matveev, O.G. Rybchenko, E.V. Tatyanin, I.I. Zverkova, J. Metastab. Nanocryst. Mater. **24**, 69 (2005).
[24] P. Henits, Á. Révész, A.P. Zhilyaev, Zs. Kovács, J. Alloys Comp. **461**, 195 (2008).
[25] B.B. Straumal, V. Pontikis, A.R. Kilmametov, A.A. Mazilkin, S.V. Dobatkin, B. Baretzky, Acta Mater. **122**, 60 (2017).
[26] S.D. Prokoshkin, I.Yu. Khmelevskaya, S.V. Dobatkin, I.B. Trubitsyna, E.V. Tatyanin, V.V. Stolyarov, E.A. Prokofiev, Acta Mater. **53**, 2703 (2005).
[27] C.X. Huang, G. Yang, Y.L. Gao, S.D. Wu, S.X. Li, J. Mater. Res. **22**, 724 (2007).
[28] T. Waitz, W. Pranger, T. Antretter, F.D. Fischer, H.P. Karnthaler, Mater. Sci. Eng. A **481**, 479 (2008).
[29] S. Jiang, Y. Zhang, L. Zhao, Y. Zheng, Intermetallics **32**, 344 (2013).
[30] Yu. Ivanisenko, A. Kilmametov, H. Roesner, R.Z.Valiev, Int. J. Mater. Res. **99**, 36 (2008).
[31] B.B. Straumal, A.R. Kilmametov, G.A. López, I. López-Ferreño, M.L. Nó, J. San Juan, H. Hahn, B. Baretzky, Acta Mater. **125**, 274 (2017).
[32] A. Kilmametov, Yu. Ivanisenko, B.B. Straumal, A.A. Mazilkin, A.S. Gornakova, M.J. Kriegel, O.B. Fabrichnaya, D. Rafaja, H. Hahn, Scripta Mater. **136** (2017) 46.
[33] A. Kilmametov, Yu. Ivanisenko, A.A. Mazilkin, B.B. Straumal, A.S. Gornakova, O.B. Fabrichnaya, M.J. Kriegel, D. Rafaja, H. Hahn, Acta Mater. **144**, (2018) 337.
[34] B.B. Straumal, A.R. Kilmametov, Yu. Ivanisenko, A.A. Mazilkin, R.Z. Valiev, N.S. Afonikova, A.S. Gornakova, H. Hahn, J. Alloys Comp. **735**, (2018) 2281.
[35] A.R. Kilmametov, Yu. Ivanisenko, B.B. Straumal, A.S. Gornakova, A.A. Mazilkin, H. Hahn, Metals **8**, 1 (2018).
[36] B.B. Straumal, A.R. Kilmametov, Yu. Ivanisenko, A.S. Gornakova, A.A. Mazilkin, M.J. Kriegel, O.B. Fabrichnaya, B. Baretzky, H. Hahn, Adv. Eng. Mater. **17**, 1835 (2015).
[37] Y. Ivanisenko, A. Kilmametov, H. Roesner, R.Z. Valiev, Int. J. Mater. Res. **99**, 36 (2008).
[38] B.B. Straumal, A.S. Gornakova, A.A. Mazilkin, O.B. Fabrichnaya, M.J. Kriegel, B. Baretzky, J.-Z. Jiang, S.V. Dobatkin, Mater. Lett. **81**, 225 (2012).
[39] R.Z. Valiev, I.V. Alexandrov, Y.T. Zhu, T.C. Lowe, J. Mater. Res. **17**, 5 (2002).
[40] Scientific Group Thermodata Europe (SGTE), Thermodynamic Properties of Inorganic Materials, Landolt-Börnstein Group IV (Physical Chemistry) **19**, Subvolume B Binary Systems, Part 3 Binary Systems from Cs-K to Mg-Zr, Springer Berlin / Heidelberg, 2005.
[41] T. Sato, S. Hukai, Y.C. Huang, J. Austral. Inst. Met. **5** (2), 149 (1960).
[42] P. Duwez, Trans. Am. Soc. Met. **45**, 934 (1953).
[43] D.H. Polonis, J.G. Parr, Trans. Am. Inst. Min. Met. Eng. **200**, 1148 (1954).
[43] Y.N. Gridnev, Yu.N. Petrov, V.A. Rafalovskiy, Vopr. Fiz. Met. Metalloved. AN UkrSSR Sb. Nauchn. Rabot **11**, 82 (1960) in Russian.
[45] W. Pitsch, A. Schrader, Arch. Eisenhüttenwes. **29**, 715 (1958).
[46] U. Dahmen, Acta Metall. Mater. **30**, 63 (1982).
[47] H. Kaneko, Y.C. Huang, J. Jpn. Inst. Met. **27**, 1393 (1963).
[48] V.N. Moiseev, Met. Sci. Heat. Treat. **11**, 335(1969).
[49] J.L. Murray, Bull. Alloy Phase Diagr. **2**, 32 (1981).
[50] U. Zwicker, Titan und Titanlegierungen. Springer, Berlin, 1974.
[51] S.K. Sikka, Y.K. Vohra, R. Chidambaram, Prog. Mater. Sci. **27**, 245 (1982).
[52] B.S. Hickman, J. Mater. Sci. **4**, 554 (1969).
[53] M.B. Kerber, M. Zehetbauer, E. Schafler, F.C. Spieckermann, S. Bernstorff, T. Ungar, JOM **63**, 61 (2011).
[54] A.R. Kilmametov, G. Vaughan, A.R. Yavari, A. LeMoulec, W.J. Botta, R.Z.Valiev, Mater. Sci. Eng. A **503**, 10 (2009).
[55] J.-J. Fundenberger, A. Morawiec, E. Bouzy, Solid State Phen. **105**, 37 (2005).
[56] A. Kobler, A. Kashiwar, H. Hahn, C. Kübel, Ultramicroscopy **128**, 68 (2013).
[57] D. Errandonea, Y. Meng, M. Somayazulu, D. Häusermann, Physica B **355**, 116 (2005).
[58] D.R. Trinkle, R.G. Hennig, S.G. Srinivasan, D.M. Hatch, M.D. Jones, H.T. Stokes, R.C. Albers, J.W. Wilkins, Phys. Rev. Lett. **91**, 025701 (2003).
[59] S. Banerjee, P. Mukhopadhyay, Phase transformations: examples from titanium and zirconium alloy, Elsevier, Amsterdam, 2010.
[60] A.R. Kutsar, M.N. Pavlovskii, V.V. Komissarov, JETP Lett. **35**, 108 (1982).
[61] J.C. Jamieson, Science **140**, 72 (1963).
[62] A. Jayaraman, W. Klement, G.C. Kennedy, Phys. Rev. **131**, 644 (1963).
[63] M.P. Usikov, V.A. Zilbershtein, Phys. Status Sol. A **19**, 53 (1973).
[64] H. Xia, G. Parthasarathy, H. Luo, Y.K. Vohra, A.L. Ruoff, Phys. Rev. B **42**, 6736 (1990).
[65] J.Z. Zhang, Y.S. Zhao, R.S. Hixson, G.T. Gray, L.P. Wang, U. Wataru, H. Saito, T. Hattori, J. Phys. Chem. Sol. **69**, 2559 (2008).
[66] N. Velisavljevic, S. MacLeod, H. Cynn. Titanium alloys at extreme pressure conditions. In: Titanium Alloys – Towards Achieving

Enhanced Properties for Diversified Applications. (Ed. N. Amin), InTech, 67-86, Rijeka, Croatia 2012.
[67] G.I. Nosova, N.B. D'yakonova, I.V. Lyasotskii, Metal Sci. Heat Treat. **48**, 421 (2006).
[68] V.S. Kraposhin, N.B. D'yakonova, I.V. Lyasotskii, Y. Wan, Metal Sci. Heat Treat. **48**, 421 (2006).
[69] G.I. Nosova, Phase Transformations in Titanium Alloys [in Russian], Metallurgiya, Moscow (1968).
[70] Yu.A. Bagaryatskii, G.I. Nosova, T.V. Tagunova, Dokl. Akad. Nauk SSSR **32**, 1225 (1955).
[71] P.D. Frost, W.M. Parris, L.L. Hirsh, J.R. Doig, C.M. Schwartz, Trans. Am. Soc. Metals **46**, 231 (1954).
[72] B.A. Hatt, J.A. Roberts, Acta Metall. **8**, 575 (1960).
[73] D. De Fontaine, N.E. Paton, J.C. Williams, Acta Metall. **19**, 1153 (1971).
[74] K.K. Mc Cabe, S.L. Sass, Philos. Mag. **23**, 957 (1971).
[75] I.V. Lyasotskii, N.B. D'yakonova, Yu.D. Tyapkin, Dokl. Akad. Nauk SSSR **237** (3), 81 (1977).
[76] B.W. Levinger, Trans. Am. Inst. Min. Met. Eng. **197**, 195 (1953).
[77] L.N. Guseva, L.K. Dolinskaya, Izv. Akad. Nauk SSSR Met. **6**, 195 (1974).
[78] L.-F. Huang, B. Grabowski, E. McEniry, D.R. Trinkle, J. Neugebauer, Phys. Status Solidi B **252**, 1907 (2015).
[79] A.V. Dobromyslov, V.A. Elkin, Scripta Mater. **44**, 905 (2001).
[80] A.V. Dobromyslov, V.A. Elkin, Mater. Sci. Eng. A **438**, 320 (2006)
[81] T. Ungar, E. Schafler, P. Hanak, S. Bernstorff, M. Zehetbauer, Mater. Sci. Eng. **462**, 398 (2007).
[82] T. Ungár, E. Schafler, P. Hanák, S. Bernstorff, M. Zehetbauer, Zeitschrift Metallkd. **96**, 578 (2005).
[83] L. von Bertalanffy, Science **111**, 23 (1950).
[84] D.A. Molodov, B.B. Straumal, L.S.Shvindlerman, Scripta Metall. **18**, 207 (1984).
[85] B.B. Straumal, L.M. Klinger, L.S. Shvindlerman, Scripta Metall. **17**, 275 (1983).
[86] G.A. López, E.J. Mittemeijer, B.B. Straumal, Acta Mater. **52**, 4537 (2004).
[87] A.S. Gornakova, S.I. Prokofiev, K.I. Kolesnikova, B.B. Straumal, Russ. J. Non-Ferrous Met. **56**, 229 (2016).
[88] A.S. Gornakova, S.I. Prokofiev, B.B. Straumal, K.I. Kolesnikova, Russ. J. Non-Ferrous Met. **57**, 703 (2016).